Nanoscale

PAPER

View Article Online
View Journal | View Issue

Cite this: *Nanoscale*, 2014, **6**, 1453

Highly flexible, transparent and self-cleanable superhydrophobic films prepared by a facile and scalable nanopyramid formation technique

Jeong-Ho Kong,[a] Tae-Hyun Kim,[a] Ji Hoon Kim,[a] Jong-Kweon Park,[b] Deug-Woo Lee,[ac] Soo-Hyung Kim[ac] and Jong-Man Kim*[ac]

A facile and scalable technique to fabricate optically transparent, mechanically flexible and self-cleanable superhydrophobic films for practical solar cell applications is proposed. The superhydrophobic films were fabricated simply by transferring a transparent porous alumina layer, which was prepared using an anodic aluminium oxidation (AAO) technique, onto a polyethylene terephthalate (PET) film with a UV-curable polymer adhesive layer, followed by the subsequent formation of alumina nano pyramids (NPs) through the time-controlled chemical etching of the transferred porous alumina membrane (PAM). It was found experimentally that the proposed functional films can ensure the superhydrophobicity in the Cassie–Baxter wetting mode with superior water-repellent properties through a series of experimental observations including static contact angle (SCA), contact angle hysteresis (CAH), sliding behaviour on the tilted film, and dynamic behaviour of the liquid droplet impacting on the film. In addition to the superior surface wetting properties, an optical transmittance of ~79% at a light wavelength of 550 nm was achieved. Furthermore, there was no significant degradation in both the surface wetting properties and morphology even after 1500-cycles of repetitive bending tests, which indicates that the proposed superhydrophobic film is mechanically robust. Finally, the practicability of the proposed self-cleanable film was proven quantitatively by observing the changes in the power conversion efficiency (PCE) of a photovoltaic device covering the film before and after the cleaning process.

Received 30th August 2013
Accepted 30th October 2013

DOI: 10.1039/c3nr04629j

www.rsc.org/nanoscale

1. Introduction

Recently, nature-inspired artificial superhydrophobic surfaces have attracted significant attention for their potential applications based on their unique and desirable surface functions, such as self-cleaning, water-repellent properties, anti-sticking, anti-icing, *etc*.[1–4] Therefore, a number of the attempts have been carried out to realize micro/nano-textured surfaces by adopting a range of fabrication techniques including the lithographic process,[5–7] micro/nano-templating,[8–11] etching,[12–16] sol–gel process,[17–20] layer-by-layer deposition,[21–23] self-assembly,[24–27] electrospinning,[28–30] laser ablation,[31–33] and hydrothermal synthesis[34–36] on various substrates, because the wetting properties of such surfaces are governed mainly by the surface geometry and can be controlled by modifying the geometry. On the other hand, many of the fabrication techniques employed thus far require strict fabrication conditions to control the surface morphology, long processing times, and specialized and/or expensive equipment. In some approaches, a degree of freedom in selecting of the base substrate is limited in the case that the surface structures are realized by the specified chemical reactions with the substrate material, and a high-temperature process is required. In addition, complexity in fabrication is unavoidable when lithographic processes are used to define the nano-scale surface geometry. Some approaches are only applicable to small areas due to uniformity issues, and some suffer from weak adhesion between the surface textures and substrates, which actually restrict their practical use. Recently, the optical transparency of the superhydrophobic surfaces was considered an important property with superior surface wettability because the desirable property can open up the possibility for expanding the applicability of the superhydrophobic surfaces by making it possible to be applied to glass-based substrates, such as building windows, solar cell panels, windshields, *etc*.[11,15,18,22,26,37,38] Furthermore, if optically transparent superhydrophobic surfaces can be produced on mechanically flexible substrates such as a film-type materials, they can potentially be employed on any curved surfaces, resulting in much wider practical applications. Unfortunately, there are only a few reports dealing with functional superhydrophobic surfaces ensuring both optical transparency and mechanical

[a]*Department of Nanofusion Technology, Pusan National University, Busan 609-735, Republic of Korea. E-mail: jongkim@pusan.ac.kr*

[b]*Nano Convergence and Manufacturing Systems Research Division, Korea Institute of Machinery and Materials (KIMM), Daejeon 305-343, Republic of Korea*

[c]*Department of Nanomechatronics Engineering, Pusan National University, Busan 609-735, Republic of Korea*

flexibility.[7,16,39] This may stem mainly from the difficulties in fabrication with a consideration of the process compatibility. Moreover, most of them still suffer from the need for elaborate/complicated processes, specialized expensive equipment, and sometimes elevated process temperatures to create the surface structures.

This paper proposes a facile and scalable method to fabricate self-cleanable superhydrophobic films satisfying both optical transparency and mechanical flexibility requirements. Several advantageous aspects in developing superhydrophobic films are appreciable. First, flexible, transparent and non-wetting properties are simultaneously achievable, allowing wider practical applications. Second, fabrication is straightforward because there are no requirements for specific process conditions and expensive experimental setup. Third, the reproducibility and scalability of the process are achievable based on well-stabilized anodic aluminum oxidation (AAO) and chemical etching processes. Fourth, strong adhesion between the surface structures and substrates is achievable, and the proposed method can be applied easily to any transparent supporting substrates with the help of an intermediate polymeric adhesive.

2. Experimental section

2.1 Fabrication of superhydrophobic film

Fig. 1a shows the fabrication process of the superhydrophobic film proposed in this paper. The first step is to form a porous alumina membrane (PAM) that is then transferred to a polyethylene terephthalate (PET) film. Initially, a ~4 μm-thick photoresist (PR, AZ4330) layer, which serves as a sacrificial material, was formed on a 4-inch silicon wafer by a spin-coating and subsequent baking processes, followed by the deposition of a ~1 μm-thick aluminum (Al) thin-film using an electron-beam evaporation technique. Subsequently, the deposited Al layer was anodized to form PAM by a standard anodization process based on a 0.3 M oxalic acid solution in a double-jacket beaker connected to a circulator. The anodizing process was conducted at a constant voltage and temperature of 45 V and 10 °C, respectively. The processed specimen was bonded manually to an acceptor substrate, which is prepared by spin-coating the UV-curable polymeric adhesive (Norland Optical Adhesive 61, NOA 61) on a bare PET film, under slightly-pressurized conditions. The polymeric adhesive layer of the bonded specimen was then fully cured by illumination with UV light with a wavelength of 254 nm and an intensity of 10 μW cm^{-2} from the backside for 100 min using an UV chamber (Spectronics, XL-1500). Subsequently, the PAM with a residual Al layer was transferred to the acceptor substrate by removing the sacrificial PR layer in an organic solvent (acetone). The bottom barrier layer of the PAM was then exposed by fully etching the residual Al layer using an aqueous solution of copper(II) chloride ($CuCl_2$) and hydrochloric acid (HCl) at a constant temperature of 55 °C. Finally, the alumina nanopyramid (NP) structures, which were attached strongly to the fully-cured polymeric adhesive layer, were formed on the PET film through the time-controlled chemical etching of the barrier layer and inter-pore walls on the PAM in a 5 wt% aqueous phosphoric acid solution under a constant temperature of 30 °C.

2.2 Characterization of superhydrophobic film

The static contact angle (SCA) and contact angle hysteresis (CAH) of the fabricated films were measured on at least five different points for each film model using a commercially-available contact angle meter (KRÜSS, DSA 20E) equipped with a CCD camera module. Before characterization, all the films were coated conformally with a thin plasma-polymerized fluorocarbon (FC) layer based on a continuous C_4F_8 glow discharge to enhance the wetting properties by reducing the surface free energy. The sliding behavior of a water droplet on a tilted surface was observed while recording the process in real time using a high-speed digital video camera (Kodak, SR-Ultra-C) capable of a maximum frame rate of 10 000 frames per s. To examine the dynamic impact behavior of the water droplet impinging on the film, the fabricated film (S5 model) was first placed on a precisely-leveled flat stage built in the contact angle meter and a 10 μL water droplet was dispensed using the syringe at a height of ~50 mm from the film surface. The dynamic behavior of the falling-and-rebounding water droplet on the surface was also observed carefully using a high-speed digital video camera. The optical properties of the fabricated films were characterized by measuring the transmittance over visible light wavelength ranging (350 to 800 nm) before and after the hydrophobic coating by UV visible spectroscopy (SCINCO, S310). The cyclic bending test was conducted using a tensile test system (JISC, JSV-H1000) at a crosshead speed of 20 mm min^{-1}.

2.3 Fabrication and characterization of dye-sensitized solar cells (DSSCs)

The DSSCs were prepared using the procedures previously reported by the authors.[40,41] Briefly, commercially-available TiO_2 nanoparticles (T25, Degussa; T240, Sigma Aldrich) were used without further treatment. To prepare the TiO_2 nanoparticle paste for the screen-printing process, TiO_2 nanoparticles (6 g), ethanol (15 g), acetic acid (CH_3COOH, 1 mL), and terpineol (20 g) were mixed in a vial and sonicated for 1 h. A solution of ethylcellulose (3 g) dissolved in ethanol (27 g) was prepared separately and then added to the TiO_2 nanoparticle-dispersed solution, which was then sonicated for 30 min. As a photoelectrode layer, the TiO_2 nanoparticle-accumulated thin layer was applied *via* a screen-printing process on a fluorine-doped tin oxide (FTO) glass (Pilkington, SnO_2:F, 7 Ω per sq.) substrate with a photoactive area of 0.6 × 0.6 cm^2. The resulting TiO_2 nanoparticle-accumulated layer formed on the FTO glass substrate *via* the screen-printing process was then sintered in an electric furnace at 500 °C for 30 min and subsequently immersed in anhydrous ethanol containing 0.3 mM of Ru–dye $(Bu_4N)_2[Ru(Hdcbpy)_2–(NCS)_2]$ (Solaronix, N719 dye) for 24 h at room temperature to allow the dye molecules to attach themselves to the entire surface of the TiO_2 nanoparticles. The dye-soaked TiO_2-nanoparticle-based photoelectrode was then rinsed with ethanol and dried in a convection oven at 80 °C for

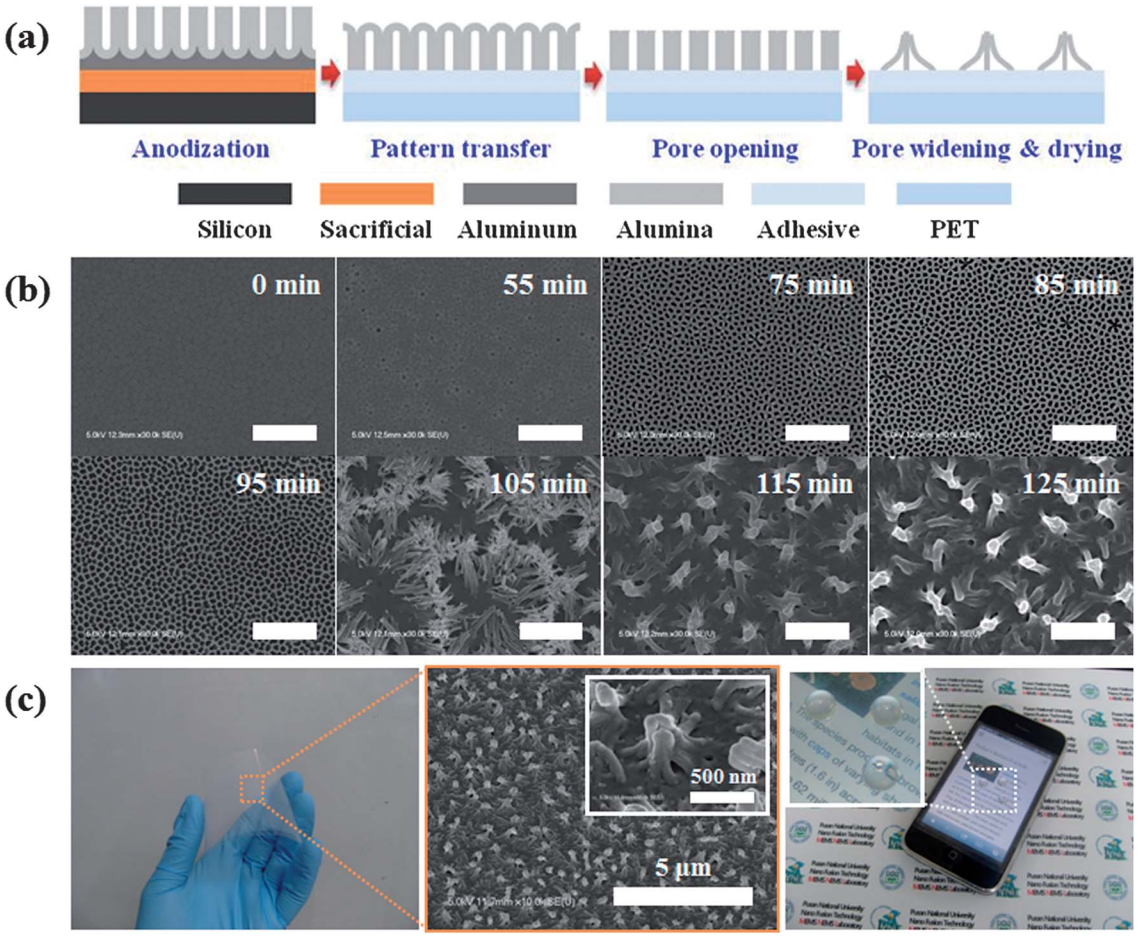

Fig. 1 Fabrication of the proposed flexible, transparent and self-cleanable superhydrophobic films. (a) Fabrication procedures, (b) surface morphology due to the etching time variations of the PAMs (scale bar: 1 μm), and (c) fabrication results.

10 min. As a counter electrode, platinum (Pt)-coated FTO glass was prepared using an ion sputter (Hitachi, E1010) operated at 2.5 kV. Both the dye-soaked TiO_2 nanoparticle-based photoelectrode and the Pt-coated counter electrode were sealed together with a 60 μm-thick hot-melt polymer film (DuPont, Surlyn) that was inserted between them, and an iodide-based liquid electrolyte (Solaronix, AN-50) was then injected into the interspace between the electrodes. The photovoltaic properties of the DSSCs were measured using a commercially-available solar simulator (Peccell, PEC-L12) under AM 1.5 illumination condition (100 mW cm^{-2}).

2.4 Self-cleaning test

The practical self-cleaning test was conducted by the following procedures. (1) First, dust particles were sprayed randomly onto the prepared self-cleanable film. Commercially-available carbon black nanoparticles (Cabot, Black Pearls 2000) with a mean diameter of ~50 nm were used as the dust with no further treatments. (2) DI water droplets (60 mL in volume) were then applied to the contaminated film, which was tilted by ~10° with a hand-made tilting system equipped with a goniometer, using a syringe. In this case, the tilting angle was determined with consideration of the CAH value obtained from the fabricated self-cleanable film. A short baking step was included to remove the water components remaining on the cleaned film. (3) Finally, the photovoltaic performance of the DSSC was characterized and compared after carefully covering the as-prepared, contaminated and cleaned film at each step using the solar simulator.

3. Results and discussion

The surface wetting properties and optical transparency of the film depend strongly on their surface morphology. In particular, the surface geometry of the superhydrophobic film proposed in this paper was determined mainly by the chemical etching step of the PAM. Therefore, the changes in the surface morphology due to the etching time variations of the PAM were first examined to determine the optimized experimental conditions by field emission scanning electron microscopy (FE-SEM; HITACHI, S4700), as shown in Fig. 1b. Initially, the emboss-like barrier layer of the PAM appeared after removing the residual Al layer. The nano-scale pores were then found on the surface after an etching time of ~55 min, and the pore size increased gradually with further increases in the etching time of the PAM.

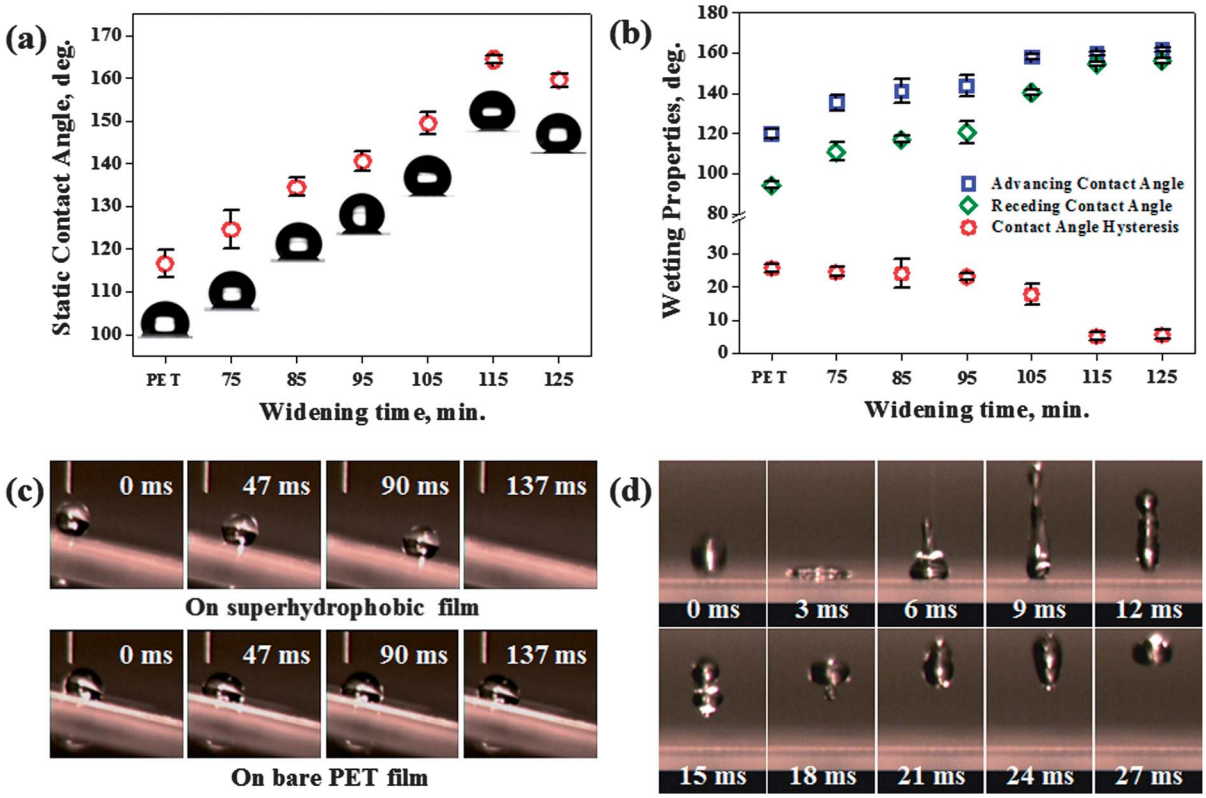

Fig. 2 Surface wetting properties measured on the fabricated superhydrophobic films. (a) SCAs and (b) CAHs variation due to the etching time variations of the PAMs, (c) water droplet sliding test results, and (d) water droplet impacting test results.

When the etching time reached ~115 min, the barrier layer was removed completely and the inter-pore sidewalls also tended to crumble, resulting in the formation of nano-scale alumina pillars. As a consequence of the assembly of the several adjacent nano-pillars, the NP structures were formed successfully on the surface, as shown in Fig. 1b. On the other hand, excessive

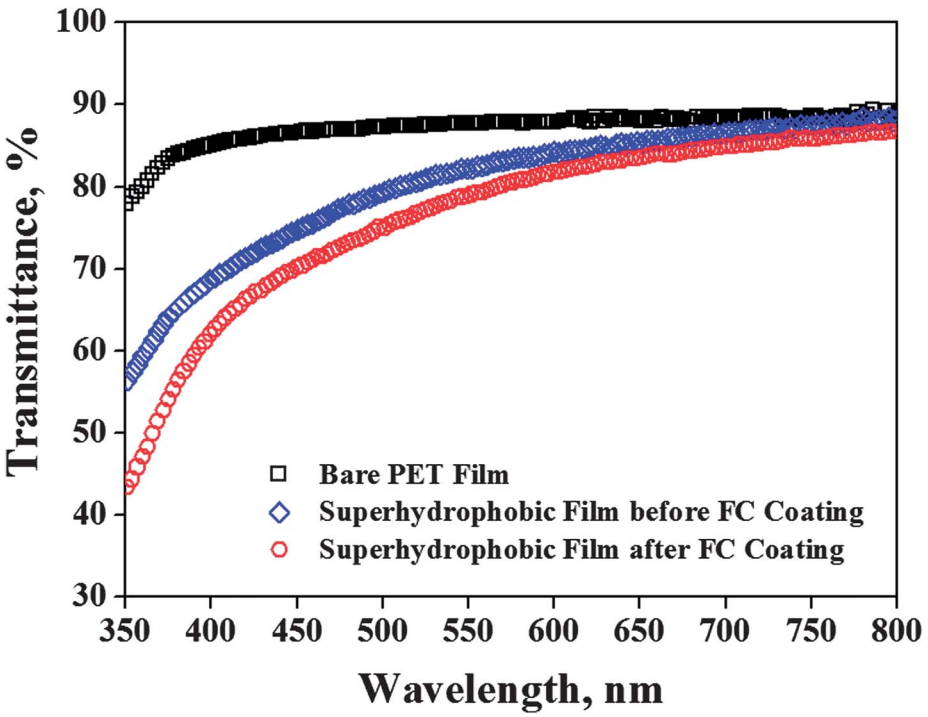

Fig. 3 Optical transmittance of the fabricated superhydrophobic film at a wavelength ranging from 350 to 800 nm.

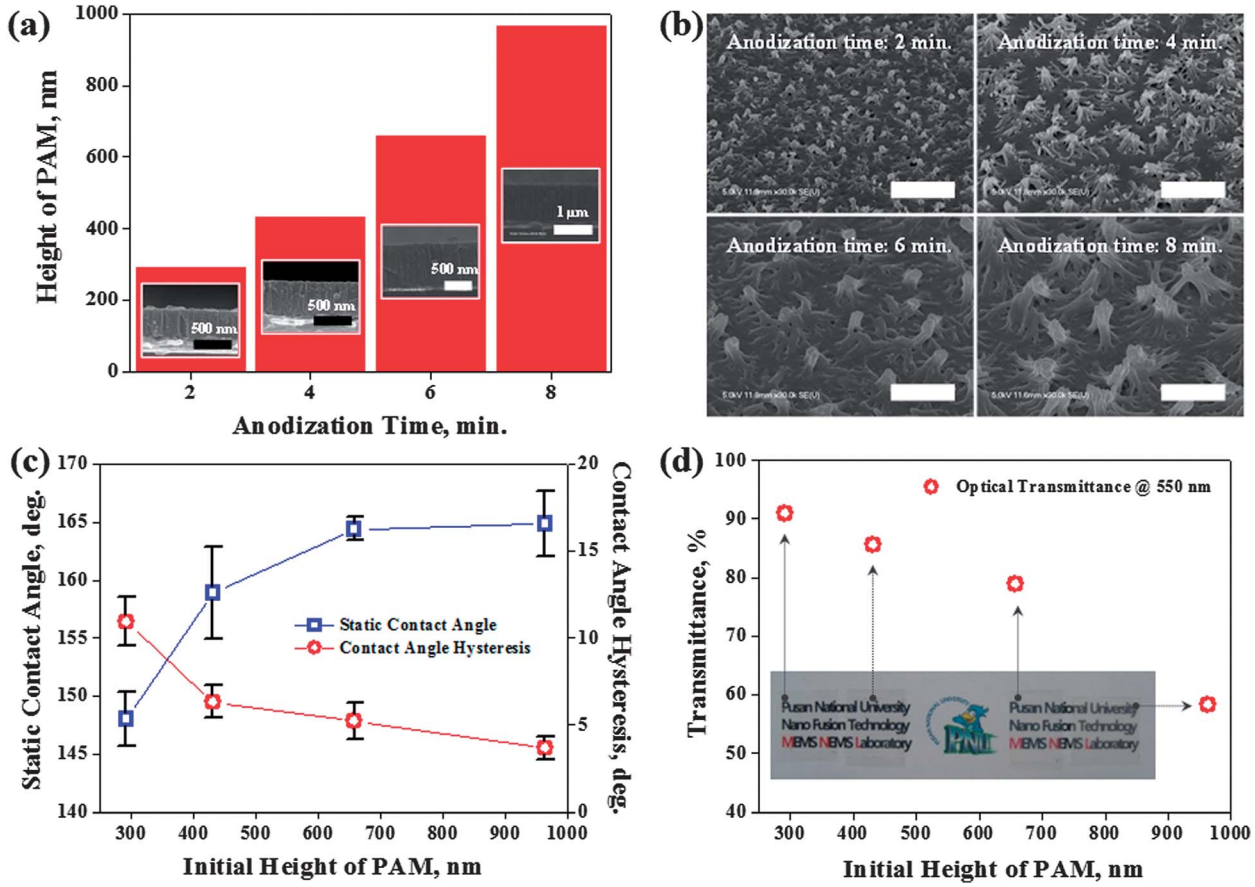

Fig. 4 Surface wetting properties and optical transmittance due to the initial height variations of the PAMs. (a) Initial heights of the PAMs resulting from the different anodization times (insets: cross-sectional SEM images for each height), (b)–(d) surface morphologies (scale bar: 1 μm), surface wettabilities (SCAs and CAHs), and optical transmittance at 550 nm wavelength of the processed surfaces with the different initial PAM heights, respectively.

etching can lead to severe structural distortion of the alumina NPs, resulting in performance degradation of the film. With the optimized etching time of the PAM, a functional film decorated with the arrayed alumina NPs was fabricated successfully, as shown in Fig. 1c. In Fig. 1c, the flexible, transparent and hydrophobic properties of the fabricated film were clearly

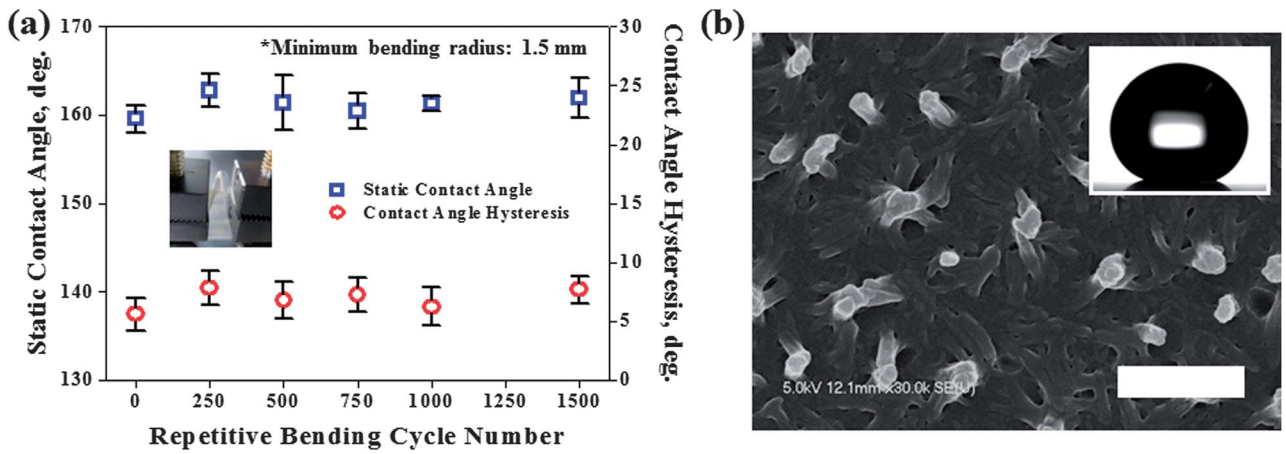

Fig. 5 Cyclic bending test. (a) SCAs and CAHs after the repetitive bending cycles with a bending radius of 1.5 mm, and (b) SEM images of the superhydrophobic surface after 1500 repetitive bending/releasing cycles (scale bar: 1 μm) (inset: digital image of the water droplet sitting on the surface after the bending test).

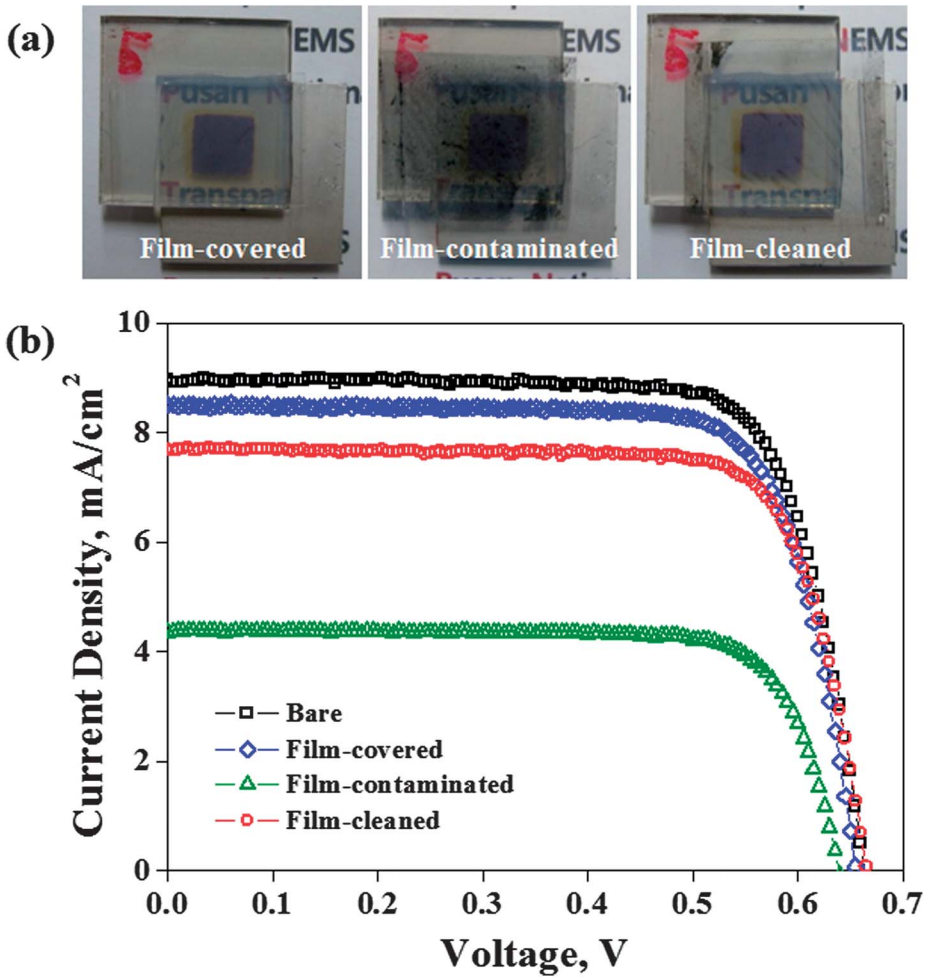

Fig. 6 Solar cell applications. (a) Digital images of the DSSC covered with a superhydrophobic film with different surface conditions (as-prepared, contaminated and cleaned), and (b) *J*–*V* curves obtained from DSSCs under the different film conditions.

Table 1 Photovoltaic characteristics measured on the DSSC under different film conditions

	J_{sc} (mA cm^{-2})	V_{oc} (V)	FF	PCE (%)
Bare	8.98	0.66	0.74	4.39
Film-covered	8.53	0.66	0.73	4.10
Film-contaminated	4.38	0.64	0.77	2.14
Film-cleaned	7.73	0.67	0.74	3.82

demonstrated. The surface morphology of the fabricated film was characterized precisely by SEM. Fig. 1c shows that the alumina NPs structures are very similar to the result in Fig. 1b (etching time of 115 min) and were distributed quite uniformly over the surface. It is worthy of note that the geometrical similarity of the surface structures was also found on repeated trials under fixed whole experimental conditions, which means that process repeatability can be achieved with the proposed fabrication methodology. In addition, the root of each NP was stuck firmly to the fully-cured adhesive layer, as shown in Fig. 1c (inset of the SEM image), which suggests that the excellent adhesion between the surface structures and the base substrate can also be ensured.

The surface wettability of the fabricated superhydrophobic films was first examined by measuring the SCAs and CAHs. First, the SCAs were measured on the films fabricated with different surface morphologies for comparison; the bare PET film, and PET films decorated with nano-structures for different PAM etching times of 75, 85, 95, 105, 115 and 125 min (hereafter, each film is denoted as S1, S2, S3, S4, S5 and S6, respectively.). Fig. 2a shows the SCAs measured on each film model with a deionized (DI) water droplet, 10 μL in volume. Although the static wetting properties were improved on all surface models with respect to that of the intrinsic PET film (116.7 ± 3.2°) due to the surface geometry effect, the highest SCA of 164.4 ± 1.0° was achieved on the S5 surface model, as shown in Fig. 2a. This suggests that the optimized surface morphology of the S5 model leads to the largest decrease in the fraction of solid/liquid interfaces beneath the water droplet by minimizing the actual contact area of the water droplet on the surface structures. The rolling-off properties of the water droplet placed on the fabricated films were also examined by measuring the CAHs for each film model. In this case, the CAH values were

obtained by calculating the differences in the advancing and receding CAs measured on each model while switching the increase and decrease in water volume sequentially. Fig. 2b shows the CAHs measured on each film model. As shown in Fig. 2b, the lowest CAH value of $5.2 \pm 1.1^\circ$ among the prepared surfaces, which indicates ~5 fold enhancement compared to that of the intrinsic model ($25.6 \pm 1.3^\circ$), was also observed on the S5 model. Further study of the rolling-off properties of the S5 surface model was conducted by observing the sliding behavior of a water droplet on a surface tilted initially by ~10°. As shown in Fig. 2c, the water droplet (10 μL) released from the nozzle of the syringe began rolling immediately over the tilted surface of the S5 model and disappeared within 137 ms, whereas the water droplet remained on the surface of the PET substrate after the droplet was released. This result clearly verifies the fact that the largest air-pocket, which can support the water droplet sufficiently, is provided on the film decorated with the geometrically optimized alumina NPs, due to the minimized actual contact area at the solid/liquid interface, as mentioned above. Consequently, this indicates that the proposed superhydrophobic film is suitable for a range of applications that requires a self-cleaning effect because it behaves in the slippery Cassie–Baxter wetting mode. In addition, the dynamic impact behavior of the water droplet impinging on the surface of the proposed superhydrophobic film was examined to evaluate the water-repellency, which is as important as the static wetting property in practical applications emphasizing the anti-wetting property. Fig. 2d shows sequential images of the water droplet impacting on the surface, which were extracted from the recorded video every 3 ms. The water droplet was first deformed and flattened maximally into a disc shape in ~3 ms after impacting at its speeding stage, which then bounced back completely from the surface in ~12 ms (contact time: ~9 ms) without fragmenting severely into smaller droplets and leaving any anchored portion of the droplet on the impact region, as shown in Fig. 2d. This suggests that the air-pocket prevents the surface from being wetted despite the impact of the water droplet. The bouncing continued several times until the water droplet came to rest by fully consuming its initial potential energy. This result clearly provides an evidence for the fact that the proposed method is very useful for realizing the functional surfaces, ensuring superhydrophobicity in the Cassie–Baxter wetting regime, even under the dynamic conditions.

The superhydrophobic surfaces should be optically transparent to be applied practically to building windows, windshields, solar cell panels, *etc.* Fig. 3 shows the transmittance curves obtained from the prepared bare PET and superhydrophobic films. The transmittance of the reference surface (bare PET) was measured to be approximately 88% at a wavelength of 550 nm. The transmittance of the reference film was decreased to ~82% at the same wavelength after being decorated with the alumina NPs (S5 surface) due to the scattering effect on nano-scale surface roughness, whereas it became slightly less transparent after the hydrophobic FC coating (~79% @ 550 nm). On the other hand, severe degradation of the transparent properties was not observed on the superhydrophobic film, despite the fact that the intermediate adhesive layer with NPs was additionally stacked on the bare PET film. This indicates that the alumina NPs optimized geometrically are useful for reducing the transparency loss in the visible range as well as for obtaining the superior surface wetting properties by producing the valleys, which can play an important role in both reducing the light loss on its travelling path and providing sufficient air-pocket sites compared to the densely-packed surface geometries, respectively.

Both the surface wetting property and optical transparency of superhydrophobic films were influenced strongly by their surface morphology. A decrease in the size of the surface structure would be desirable for obtaining better optical transparency by minimizing the light scattering on the surface. On the other hand, in this case, the surface wetting properties will be degraded accordingly by allowing the water droplet to penetrate to the bottom surface more easily due to the surface structures with a low aspect ratio. To evaluate the surface condition ensuring good performance in both properties, a parameter study was carried out on the films with different-sized surface structures. In the proposed fabrication strategy, the size of the surface structures on the film can be determined easily by controlling the initial height of the PAM with different anodization times. Fig. 4a shows the changes in the heights of the PAMs due to anodization time variations (inset figures show the cross-sectional SEM images of the PAMs). The PAM heights increased gradually with increasing anodization time, as shown in Fig. 4a. The SEM images of the corresponding surface geometries of the films at different anodization times of 2, 4, 6 and 8 min were also shown in Fig. 4b. These results show that larger NP-shaped surface structures were obtained for the film with a higher initial PAM. Fig. 4c and d show the measured wetting properties (SCAs and CAHs) and optical properties (transmittance @ 550 nm) of each film with different initial heights of PAMs (*e.g.* different surface morphologies). As expected, the best surface wetting property was observed on the film with the highest initial PAM among the films, whereas the poorest optical properties were also found due to a significant amount of light scattering on the surface textured with the largest NPs. This trade-off relationship between the surface wetting and optical properties was clearly observed in Fig. 4c and d. These experimental observations verify the fact that the films with an initial PAM height ranging from approximately 400 to 700 nm (here, F2 and F3 films) can provide the feasibility to be utilized as a self-cleanable film in practical glass-based applications based on their superior wetting properties and moderate optical property. In addition to the superior surface wetting properties, mechanical flexibility and optical transparency, the structural stability of the superhydrophobic surface against various mechanical deformation conditions is also an important factor that should be considered for practical applications. A cyclic bending test was conducted with a bending radius of curvature of ~1.5 mm to confirm the effectiveness of the proposed superhydrophobic film in terms of the mechanical robustness. The corresponding SCAs and CAHs of the film were measured every 250th cycle through repetitive bending cycles. Fig. 5a shows the changes in the SCAs and CAHs

of the film under 1500 repetitive bending cycles. The fabricated films showed no significant degradation of the surface wetting properties, even under severe repetitive bending deformation. Moreover, no prominent structural distortion such as cracks and detachment were observed on the film tested under the same conditions, as shown in Fig. 5b. This verifies that the proposed superhydrophobic film can be used multiple times on the curved surfaces, maintaining its functionality.

To show the practicability of the proposed transparent superhydrophobic film, the self-cleaning effect was evaluated by characterizing the photovoltaic performance of a dye-sensitized solar cell covered with the fabricated film before and after the cleaning process. Fig. 6a shows the digital images of the DSSC covered with the film under the different conditions (as-prepared, contaminated and cleaned). A naked eye observation showed that most of the dust particles sprayed on the film has been washed after the cleaning process. The current density–voltage (J–V) curves obtained from the DSSC under the different film conditions are shown in Fig. 6b, and the measured photovoltaic characteristics were also summarized in Table 1. The initial power conversion efficiency (PCE) value measured on the bare DSSC was 4.39%, whereas it decreased slightly to 4.1% after covering the as-prepared superhydrophobic film due to the optical loss of the light transmitted through the film. The PCE value of the DSSC covered with the as-prepared film decreased severely to 2.14% after being contaminated with dust particles. In particular, it must be noted that the current density (J_{sc}) value of the DSSC covered with the contaminated film was decreased by 48.7% (from 8.53 to 4.38 mA cm^{-2}), while maintaining a similar open-circuit voltage (V_{oc}) and fill factor (FF) compared to those of the DSSC covered with the as-prepared film. This means that the dust particles are the main contributors for degrading the photovoltaic performance of the DSSC by blocking the incident light significantly. After the cleaning process, the J_{sc} value measured on the DSSC covered with the cleaned film increased to 7.73 mA cm^{-2} and the corresponding PCE was 3.82%, which means that the photovoltaic performance of the DSSC had recovered 93.2% with respect to that of the DSSC covered with the as-prepared film. In comparison, the PCE of the DSSC without covering the self-cleanable film was recovered only 46.1% compared to that of the as-fabricated DSSC even after experiencing the same cleaning process. These results suggest that further optimization of the surface geometry would make it possible for the proposed superhydrophobic film to be considered as a self energy-saving method by recovering the energy efficiency.

4. Conclusion

In summary, a highly flexible, transparent and self-cleanable superhydrophobic film with the structural robustness was demonstrated successfully using a simple and scalable non-lithographic process. The surface geometry of the proposed superhydrophobic film could be optimized simply by controlling the chemical etching time of the PAM transferred to the PET substrate with an intermediate polymeric adhesive. The superior superhydrophobicity of the proposed film was confirmed by a series of experimental investigations including SCA, CAH, sliding and impact tests. Highly transparent properties comparable to those of the bare PET were also achieved on the proposed superhydrophobic film. In addition, the proposed film showed structural robustness with no significant degradation of its superhydrophobic performance and surface morphology after a cyclic bending/releasing test. Based on these properties, the self-cleaning ability of the proposed film was studied quantitatively with the photovoltaic devices. In detail, the cell efficiency of the photovoltaic device contaminated with dust particles was recovered efficiently to ~93.2% with respect to its initial value with the help of the self-cleanable film. These achievements clearly suggest that the proposed superhydrophobic film is potentially feasible to be implemented in a wide range of the practical applications owing to its desirable properties including mechanical flexibility, optical transparency, and mechanical robustness as well as superior surface wetting properties.

Acknowledgements

This work was supported by "Development of Next Generation Multi-functional Machining Systems for Eco/Bio Components" project of Ministry of Knowledge Economy.

Notes and references

1 Y.-L. Zhang, H. Xia, E. Kim and H.-B. Sun, *Soft Matter*, 2012, **8**, 11217.
2 X. Zhang, F. Shim, J. Niu, Y. Jiang and Z. Wang, *J. Mater. Chem.*, 2008, **18**, 621.
3 Z. Guo, W. Liu and B.-L. Su, *J. Colloid Interface Sci.*, 2011, **353**, 335.
4 X. Yao, Y. Song and L. Jiang, *Adv. Mater.*, 2011, **23**, 719.
5 J. Feng, M. T. Tuominen and J. P. Rothstein, *Adv. Funct. Mater.*, 2011, **21**, 3715.
6 T.-I. Kim, C. H. Baek, K. Y. Suh, S.-M. Seo and H. H. Lee, *Small*, 2008, **4**, 182.
7 M. Im, H. Im, J.-H. Lee, J.-B. Yoon and Y.-K. Choi, *Soft Matter*, 2010, **6**, 1401.
8 Y. Lee, K.-Y. Ju and J.-K. Lee, *Langmuir*, 2010, **26**, 14103.
9 P. Peng, Q. Ke, G. Zhou and T. Tang, *J. Colloid Interface Sci.*, 2013, **395**, 326.
10 M. Qu, G. Zhao, Q. Wang, X. Cao and J. Zhang, *Nanotechnology*, 2008, **19**, 055707.
11 M. Kim, K. Kim, N. Y. Lee, K. Shin and Y. S. Kim, *Chem. Commun.*, 2007, 2237.
12 Y. Xiu, L. Zhu, D. W. Hess and C. P. Wong, *Nano Lett.*, 2005, **7**, 3388.
13 Y. Kwon, N. Patankar, J. Choi and J. Lee, *Langmuir*, 2009, **25**, 6129.
14 S. Dash, M. T. Alt and S. V. Garimella, *Langmuir*, 2013, **28**, 9606.
15 K.-C. Park, H. J. Choi, C.-H. Chang, R. E. Cohen, G. H. Mckinley and G. Barbastathis, *ACS Nano*, 2012, **6**, 3789.
16 A. D. Tserepi, M.-E. Vlachopoulou and E. Gogolides, *Nanotechnology*, 2006, **17**, 3977.

17 R. Taurino, E. Fabbri, M. Messori, F. Pilati, D. Pospiech and A. Synytska, *J. Colloid Interface Sci.*, 2008, **325**, 149.
18 S. A. Mahadik, M. S. Kavale, S. K. Mukherjee and A. V. Rao, *Appl. Surf. Sci.*, 2010, **257**, 333.
19 D. Su, C. Huang, Y. Hu, Q. Jiang, L. Zhang and Y. Zhu, *Appl. Surf. Sci.*, 2011, **258**, 928.
20 Y.-T. Peng, K.-F. Lo and Y.-J. Juang, *Langmuir*, 2010, **26**, 5167.
21 K.-S. Liao, A. Wan, J. D. Batteas and D. E. Bergbreiter, *Langmuir*, 2008, **24**, 4245.
22 Y. Li, F. Liu and J. Sun, *Chem. Commun.*, 2009, 2730.
23 Y. Zhao, M. Li, Q. Lu and Z. Shi, *Langmuir*, 2008, **24**, 12651.
24 Y. Horiuchi, K. Fujiwara, T. Kamegawa, K. Mori and H. Yamashita, *J. Mater. Chem.*, 2011, **21**, 8543.
25 M. A. Raza, E. S. Kooij, A. v. Silfhout and B. Poelsema, *Langmuir*, 2010, **26**, 12962.
26 Y. Rahmawan, L. Xu and S. Yang, *J. Mater. Chem. A*, 2013, **1**, 2955.
27 S. Pechook and B. Pokroy, *Adv. Funct. Mater.*, 2012, **22**, 745.
28 S. J. Hardman, N. M.- Sarih, H. J. Riggs, R. L. Thompson, J. Rigby, W. N. A. Bergius and L. R. Hutchings, *Macromolecules*, 2011, **44**, 6461.
29 M. Ma, M. Gupta, Z. Li, L. Zhai, K. K. Gleason, R. E. Cohen, M. F. Rubner and G. C. Rutledge, *Adv. Mater.*, 2007, **19**, 255.
30 X. Wang, B. Ding, J. Yu and M. Wang, *Nano Today*, 2011, **6**, 510.
31 J. Yong, F. Chen, Q. Yang, D. Zhang, H. Bian, G. Du, J. Si, X. Meng and X. Hou, *Langmuir*, 2013, **29**, 3274.
32 E. Fadeeva, V. K. Truong, M. Stiesch, B. N. Chichkov, R. J. Crawford, J. Wang and E. P. Ivanova, *Langmuir*, 2011, **27**, 3012.
33 A. Stojanovic, G. R. J. Artus and S. Seeger, *Nano Res.*, 2010, **3**, 889.
34 J. Wu, J. Xia, W. Lei and B. Wang, *PLoS One*, 2010, **5**, e14475.
35 X. Liu and J. He, *Langmuir*, 2009, **25**, 11822.
36 F. Guo, X. Su, G. Hou, Z. Liu and Z. Mei, *Colloids Surf., A*, 2012, **395**, 70.
37 X. Deng, L. Mammen, Y. Zhao, P. Lellig, K. Müllen, C. Li, H.-J. Butt and D. Vollmer, *Adv. Mater.*, 2011, **23**, 2962.
38 S. Manakasettharn, T.-H. Hsu, G. Myhre, S. Pau, J. A. Taylor and T. Krupenkin, *Opt. Mater. Express*, 2012, **2**, 159797.
39 H. Budunoglu, A. Yildirim, M. O. Guler and M. Bayindir, *ACS Appl. Mater. Interfaces*, 2011, **3**, 539.
40 J. Y. Ahn, H. K. Cheon, W. D. Kim, Y. J. Kang, J.-M. Kim, D.-W. Lee, C. Y. Cho, Y. H. Hwang, H. S. Park, J. W. Kang and S. H. Kim, *Chem. Eng. J.*, 2012, **188**, 216.
41 J. Y. Ahn, J. H. Kim, K. J. Moon, J. H. Kim, C. S. Lee, M. Y. Kim, J. W. Kang and S. H. Kim, *Sol. Energy*, 2013, **92**, 41.